Chinese Chemical Letters 37 (2026) 112102

Contents lists available at ScienceDirect

Chinese Chemical Letters

journal homepage: www.elsevier.com/locate/cclet

Engineered tetrahedral framework nucleic acids (tFNAs): Modification strategies and biomedical applications

Tingting Zuo[a,1], Tao He[b,1], Yuan Gao[c], Siyi Yang[b], Yun Wang[b], Zhengyang Yang[d,*], Chao Zhang[e,*], Yunfeng Lin[b,*]

[a] College of Biological Sciences and Technology, Yili Normal University, Xinjiang Key Laboratory of Lavender Conservation and Utilization, Yining 835000, China
[b] State Key Laboratory of Oral Diseases, National Center for Stomatology, National Clinical Research Centre for Oral Diseases, West China Hospital of Stomatology, Sichuan University, Chengdu 610041, China
[c] Department of Gastroenterology and Hepatology, Digestive Endoscopy Medical Engineering Research Laboratory, West China Hospital, Sichuan University, Chengdu 610041, China
[d] Department of General Surgery, Beijing Friendship Hospital, Capital Medical University, Beijing 100050, China
[e] Department of Oncology, Zhujiang Hospital, Southern Medical University, Guangzhou 510282, China

ARTICLE INFO

Article history:
Received 25 July 2025
Revised 10 November 2025
Accepted 11 November 2025
Available online 12 November 2025

Keywords:
Tetrahedral framework nucleic acids
DNA nanotechnology
Functionalization strategies
Biomedical applications
Therapeutics
Diagnostics

ABSTRACT

Tetrahedral framework nucleic acids (tFNAs) have emerged as a promising platform for a wide range of biomedical applications due to their unique structural stability, ease of synthesis, and excellent biocompatibility. This review provides a comprehensive overview of the various modification strategies for tFNAs, including vertex modification, edge functional loading, internal encapsulation, and surface coating. These modifications enable precise control over their biological activity, facilitating advancements in drug delivery, gene therapy, tissue engineering, and diagnostic imaging. Additionally, the structural engineering of tFNAs has enabled their integration into theranostic platforms, offering significant potential for personalized medicine. The review also discusses the challenges involved in the clinical translation of tFNAs, such as scalability, pharmacokinetic optimization, and regulatory approval, and presents a forward-looking perspective on the emerging trends that could further broaden the scope of tFNAs in clinical applications. Finally, we conclude by outlining the future prospects of tFNAs in next-generation therapeutic and diagnostic systems, highlighting their transformative potential in the biomedical field.

© 2026 Published by Elsevier B.V. on behalf of Chinese Chemical Society and Institute of Materia Medica, Chinese Academy of Medical Sciences.

1. Introduction

The manipulation of materials at the nanoscale has spurred significant advances across various scientific fields, particularly in the realm of DNA nanotechnology [1–9]. Leveraging the programmability, precision self-assembly, and excellent biocompatibility of DNA, researchers have been able to design and fabricate complex nanoscale structures with remarkable control over their size, shape, and function [10–17]. Among the diverse DNA nanostructures developed, tetrahedral framework nucleic acids (tFNAs) have emerged as a particularly promising class [18–23].

Firstly, these three-dimensional (3D) DNA nanostructures are constructed through the self-assembly of carefully designed DNA strands, forming a stable tetrahedral cage [24,25]. The rigid geometry of tFNAs provides exceptional structural stability, making them resistant to enzymatic degradation and environmental fluctuations, which is crucial for maintaining integrity in complex biological systems [12,20]. Secondly, one of the key advantages of tFNAs lies in their remarkable editability, which serves as the foundation for their functional modifications. This feature provides an unparalleled level of programmability, enabling the incorporation of a wide range of therapeutic, diagnostic, and targeting agents. The precise and modular functionalization of these vertices allows tFNAs to be tailored for various biomedical applications. These modifications are the foundation for the diverse functionalities of tFNAs, making them adaptable for drug delivery, gene therapy, tissue engineering, biosensing, and bioimaging. Moreover, the ability to modify both the vertices and the surface of tFNAs ensures that these structures can be engineered to meet the specific needs of various applications [26–28]. In addition to their excellent structural properties, the inherent biocompatibility of DNA makes tFNAs

* Corresponding authors.
E-mail addresses: doctoryangzy@163.com (Z. Yang), zc15996256330@smu.edu.cn (C. Zhang), yunfenglin@scu.edu.cn (Y. Lin).
[1] These authors contributed equally to this work.

https://doi.org/10.1016/j.cclet.2025.112102
1001-8417/© 2026 Published by Elsevier B.V. on behalf of Chinese Chemical Society and Institute of Materia Medica, Chinese Academy of Medical Sciences.

suitable for *in vivo* applications with minimal immunogenicity. This characteristic is essential for their use in the medical field, where compatibility with biological systems is paramount [29–31]. The unique properties and inherent programmability of engineered tFNAs have positioned them as versatile nanoplatforms for addressing key challenges in biomedical science [32,33]. Moving beyond conventional drug delivery, their capabilities are being explored in sophisticated applications such as precision gene therapy, targeted tissue engineering and regenerative medicine, highly sensitive biosensing, and advanced bioimaging [34–42].

However, the transition of tFNAs from laboratory innovations to clinical applications faces challenges, including issues related to scalability, pharmacokinetics, and regulatory approval. These challenges must be addressed to fully realize the potential of tFNAs in clinical settings [43,44]. This review will explore the various strategies for modifying tFNAs, with a focus on their potential to address key challenges in biomedicine. We will also discuss their emerging role in theranostic applications, offering a glimpse into how tFNAs could reshape the landscape of personalized medicine.

2. Design and fabrication of tFNAs

The ability to precisely engineer the structure is central to the biomedical promise of tFNAs. This section details the principles governing their design and the methods employed for their fabrication.

2.1. Basic structural design

tFNAs are 3D cage structures that represent a prime example of rationally designed and precisely fabricated DNA nanostructures [18,19,45]. Unlike simpler linear DNA duplexes, a typical DNA tetrahedron is composed of six double-helical DNA edges connected at four vertices [18,45]. This structure is typically achieved through the self-assembly of four carefully designed single-stranded DNA oligonucleotides (ssDNAs). Each ssDNA is engineered with specific complementary regions that hybridize with segments of other ssDNAs, driving the formation of the six double-helical edges and defining the overall tetrahedral configuration [46].

A critical consideration in tFNA design is the sequence-specific hybridization domain. Each strand must be engineered to minimize undesired secondary structures or misfolding while maximizing intermolecular fidelity to ensure high assembly yield and structural integrity [47,48]. Computational tools, often employed for sequence screening, predict optimal thermodynamics and folding pathways, thereby enhancing assembly efficiency [34]. Additionally, balancing strand lengths is crucial to provide sufficient structural rigidity without compromising synthesis feasibility or hybridization kinetics.

The inherent modularity of the tFNA design, particularly the presence of four well-defined vertices, is key to its programmable biofunctionalities. These vertices typically allow for the incorporation of programmable overhangs, sticky ends, or chemical handles at defined positions (usually 5′ or 3′ termini) [49]. This capability enables further structural elaboration, such as hierarchical assembly into higher-order superstructures or hybrid materials, and facilitates the site-specific conjugation of functional units like aptamers, targeting ligands, or enzyme-responsive motifs without disrupting the core geometry [50,51]. Another key design parameter is managing the angle and torsional stress at the vertices, which can significantly affect overall structural fidelity and performance in biological systems [52]. Studies have shown that adjusting sequence composition or incorporating flexible linkers at junctions can modulate these properties, ensuring tFNAs maintain structural integrity under mechanical or chemical stress, which is vital for *in vivo* applications [52]. Thus, meticulous structural design directly underpins the stability and functional capabilities of tFNAs.

2.2. Assembly mechanism and different fabrication methods

The foundation of tFNA fabrication lies in the highly specific and predictable self-assembly process driven by Watson-Crick complementary base pairing [53,54]. The standard method involves a controlled thermal annealing process: component ssDNAs are mixed, heated to a high temperature (typically 90–95 °C) to denature any pre-existing secondary structures, and then slowly cooled [55–57]. This slow cooling allows the complementary regions to find their partners and hybridize into the thermodynamically most favorable structures, which for properly designed strands, is the tFNA.

As shown in Fig. S1 (Supporting information), several fabrication methods have been developed: (1) One-pot annealing (Fig. S1a): This is the most widely used and arguably the most scalable method, in which four or more single-stranded DNAs are mixed and subjected to a defined rapid thermal annealing protocol, leading to the high-yield self-assembly of tFNAs in a single step [12,26,58]; (2) Three-way junction fabrication (Fig. S1b): This modular approach involves first assembling smaller, prefabricated Y-shaped DNA junction components and subsequent precise assembly together to form the vertices and edges of the tetrahedral framework, offering high control but can be more complex than one-pot annealing [47,59]. (3) DNA origami method (Fig. S1c): Utilizing a long scaffold strand folded into the desired shape by numerous short staple strands, DNA origami can theoretically be applied to create larger or more complex tFNA-like structures [60–62]. While it demonstrates significant potential for intricate nanoscale construction, its practical application for standard tFNAs and large-scale biomedical contexts remains less explored compared to one-pot annealing.

Among these methods, the one-pot annealing approach is currently considered the most scalable and best suited for clinical translation [20]. Its simplicity, cost-effectiveness, and compatibility with automation and good manufacturing practice (GMP) standards enable high-throughput production with relatively consistent batch quality and minimized purification requirements for certain applications [20,63].

3. Functionalization strategies and biomedical applications

Functionalization is a pivotal step in tailoring tFNAs for specific biomedical applications, involving the conjugation of various therapeutic, diagnostic, or targeting molecules to tFNAs. By integrating these functional moieties through precise structural design, engineered tFNAs possess both unique programmability and inherent biocompatibility, enabling their use as versatile nanoplatforms in diverse biomedical applications including drug delivery, tissue engineering, regenerative medicine, biosensing, and bioimaging [48,64–73].

To date, four primary functionalization strategies have been established, including vertex modification, edge functional loading, internal encapsulation, and surface coating, each enabling tailored design for specific biomedical applications (Fig. 1).

3.1. Vertex modification

The intrinsic programmability of DNA endows tFNAs with excellent editability. Notably, the four vertices of the tFNA structure serve as critical functionalization sites, where a diverse array of programmed functionalities for diverse applications-including nucleic acids, peptides, chemical groups, and metal ions-can be se-

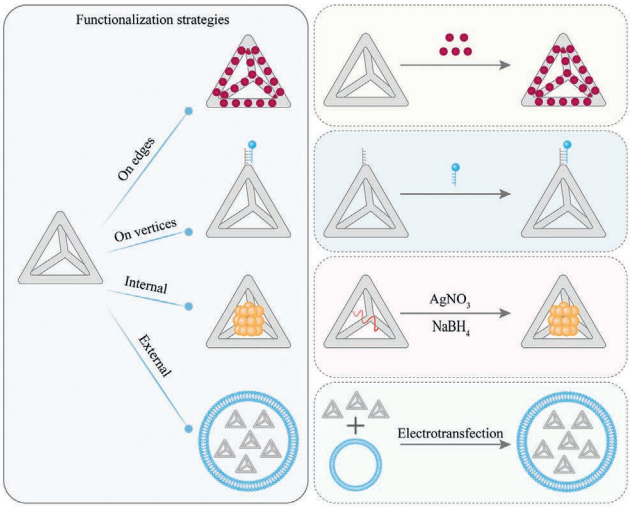


Fig. 1. Functionalization strategies of tFNAs, including modifications on vertices, modifications on edges, internal modifications, and external modifications.

lectively modified, either at individual or multiple vertices [74–83]. However, the mechanisms of conjugation vary significantly depending on the nature of the attached molecules.

For nucleic acid-based modifications such as DNA, RNA, PNA, and LNA, site-specific hybridization can be readily achieved through the Watson–Crick base pairing principle. In the earliest applications, functional nucleic acid sequences were directly extended from the phosphate backbone at the tFNA vertices [74–78]. Subsequently, to enable controlled RNA loading and unloading while preserving the structural integrity of the tFNAs, DNA aptamers were introduced at the vertices to form "tail-like" overhangs. These structures hybridize with therapeutic RNA sequences to form DNA-RNA duplexes, which can be selectively cleaved by cytoplasmic RNase H, thereby releasing RNA while leaving the tFNA carrier intact [79,80].

Peptide functionalization, in contrast, often involves covalent strategies such as click chemistry, whereby peptides are site-specifically conjugated to the vertices of tFNAs. This approach ensures precise control over both loading capacity and modification sites, while maintaining the stability of the linkage under physiological conditions [81,82].

Similarly, other organic compounds and metal ions can be functionalized at the vertices of tFNAs *via* click chemistry or other chemical reactions, offering additional flexibility for chemical modification and expanding the range of functional applications [83].

3.1.1. Drug delivery

tFNAs offer a versatile platform for co-delivery strategies, enabling the simultaneous incorporation of multiple therapeutic agents within a single nanostructure due to the capacity of various small-molecule drugs to interact with tFNAs [84–91]. Such designs often exploit tumor microenvironment characteristics, such as low pH or redox gradients, to trigger localized release [92–96]. This dual or multi-agent delivery capability is particularly useful in oncology and immunotherapy, where synergistic treatment effects are desired. For other protein-based therapies, tFNAs help overcome challenges related to stability and cellular internalization [97–100]. By integrating peptides or enzymes into the DNA framework, tFNAs can improve the bioavailability and bioactivity of otherwise unstable therapeutic agents, showing promise in treating resistant infections and modulating immune responses [101,102].

The incorporated tFNA-based systems have been explored in a wide range of therapeutic applications. As shown in Fig. S2 (Supporting information), Fan *et al.* developed an inhalable, pH-responsive tFNAs nanomachine capable of simultaneously delivering an immunomodulatory CpG oligonucleotide and a programmed cell death ligand 1 (PDL1)-targeting antagonistic DNA aptamer (CP@tFNAs) to treat metastatic lung cancer (Fig. S2a) [78]. The atomic force microscopy (AFM) results suggested the successful assembly of tFNAs, Tri-DON and DNA nanoribbon (Fig. S2b). Female C57BL/6 mice were administered with Cy5.5-labeled CP@tFNAs through the microsprayer aerosolizer (Fig. S2c). Twenty-four hours after administration, they euthanized the mice and collected the lungs for tissue fluorescence imaging (Fig. S2d) and immunofluorescence staining analysis. As exhibited in Fig. S2e, the CP@tFNAs inhalation displayed significantly stronger Cy5.5 fluorescence in the lung, with about 10 times enhancement. The lung metastatic tumor-bearing mice were then used to monitor the tumor growth (Fig. S2f). As depicted in Fig. S2g, the CP@tFNAs treatment group had the lowest fluorescence intensity in the lung area, confirming that it can significantly inhibit tumor growth.

To further enhance cell-specific targeting and therapeutic efficacy, *N*-acetylated proline-glycine-proline (Ac-PGP) peptides, known to selectively recognize the C-X-C chemokine receptor 2 (CXCR2) receptor on neutrophils, were site-specifically conjugated to the vertex of tFNAs *via* copper-free click chemistry. This covalent linkage enabled the precise spatial orientation of the targeting ligand while preserving the structural integrity of the tetrahedral framework. The resulting Ac-PGP-tFNA complex retained the hallmark features of tFNA-based nanocarriers, including excellent biocompatibility, cellular internalization efficiency, and high drug-loading capacity. By leveraging click chemistry for stable peptide immobilization, the platform achieved controlled surface modification and reduced nonspecific interactions, thereby significantly improving the selectivity and delivery efficiency toward neutrophil-mediated inflammatory microenvironments. This strategy underscores the potential of chemically engineered tFNA systems in constructing modular and multifunctional nanotherapeutics for targeted inflammation modulation and beyond [81].

In another study, as shown in Fig. S3 (Supporting information), Li *et al.* developed an interface engineering method based on tFNAs to construct spherical nucleic acids (tDF-SNAs) (Fig. S3a), with robustness in geometric shape (Figs. S3b and c). They prepared tDF-SNAs by self-assembly of the freshly formed thiolated tDFs onto the gold NP core *via* the Au-S bond (Fig. S3d). The endocytosis mechanisms of tDF-SNAs were estimated to investigate the influences of the spiky architecture on the cellular uptake process (Fig. S3e). The red fluorescence of tDF-SNAs exhibited high co-localization with both the endoplasmic reticulum and Golgi apparatus over the lysosomes (Fig. S3f) [83].

3.1.2. Tissue engineering and regenerative medicine

Bone regeneration represents one of the most extensively studied applications of tFNAs due to their ability to modulate osteogenic differentiation and inflammatory responses. A study demonstrated that the delivery of miR-335–5p-modified tFNAs *via* an injectable heparin-lithium hydrogel could effectively promote bone regeneration in steroid-associated osteonecrosis [103]. This composite hydrogel system is shown to protect the miRNA cargo while enhancing osteogenic gene expression and mineral deposition at the defect site, showing significant therapeutic potential in challenging clinical scenarios. tFNAs have also been employed as bioswitchable carriers for microRNA delivery, enabling context-responsive activation of osteogenic pathways. For instance, tFNAs carrying osteogenesis-inducing miRNAs have been shown to selectively trigger bone regeneration in response to specific microenvironmental cues [104].

Angiogenesis is essential for tissue regeneration, and tFNAs have been explored as effective tools to stimulate vascular growth

and remodeling [105]. An emerging strategy involves functionalizing tFNAs with angiogenic aptamers, such as Apt-A2, which target and activate pro-angiogenic signaling pathways in endothelial cells. Zhao *et al.* demonstrated that Apt-A2-conjugated tFNAs significantly enhanced endothelial cell proliferation, migration, and tube formation *in vitro* [84]. When tested in a murine hindlimb ischemia model, these modified tFNAs accelerated blood flow recovery and increased microvessel density at the site of injury, suggesting their potential to induce robust neovascularization *in vivo*. Another approach employed tFNAs as carriers for microRNA-126 (miR-126) mimics, which are known regulators of vascular integrity and angiogenesis. In the study by Ge *et al.* tFNA-miR-126 constructs exhibited enhanced cellular internalization and sustained miRNA release, leading to improved expression of angiogenic genes such as vascular endothelial growth factor (VEGF) and endothelial nitric oxide synthase (eNOS) in endothelial cells [106]. These nanostructures also effectively suppressed vascular inflammation, reducing the expression of adhesion molecules (*e.g.*, intercellular adhesion molecule 1 (ICAM-1), vascular cell adhesion molecular-1 (VCAM-1)) and leukocyte infiltration in vascular injury models. Importantly, *in vivo* experiments in models of vascular remodeling and homeostasis showed that these tFNA constructs promoted endothelial repair and vessel stabilization, underscoring their therapeutic potential in treating vascular diseases such as atherosclerosis or post-surgical restenosis.

3.1.3. Biosensing and bioimaging

Optical biosensors rely on optical signal changes-such as fluorescence, colorimetric shifts, or surface plasmon resonance (SPR)-to detect target molecules. The rigid and programmable structure of tFNAs facilitates precise spatial arrangement of fluorophores and quenchers, which is ideal for Förster resonance energy transfer (FRET)-based sensing. As shown in Fig. S4 (Supporting information), Chen *et al.* constructed a generally applicable DNA framework signal amplification platform (DSAP) to achieve high-sensitive detection for diverse immune cells (Fig. S4a) [44]. Conversely, the Cy5+ ratios of HuT-78 cells treated with probes from 0 to 60 min (Fig. S4b). The same trends could be observed through mean fluorescence intensity (MFI) results (Fig. S4c). In addition to remarkable sensitivity, DSAP is endowed with superior specificity compared with those constantly fluorescent probes (Figs. S4d and e).

Electrochemical biosensors harness electrical signals-typically current, voltage, or impedance changes-induced by biomolecular interactions. The surface addressability and stability of tFNAs make them suitable for modifying electrode surfaces with precise and dense recognition elements. In the study by Lin *et al.*, a tFNA-modified gold electrode surface was engineered to detect target DNA sequences with high sensitivity and specificity [107]. The uniform orientation and minimized steric hindrance of the immobilized probes enabled more efficient hybridization, resulting in femtomolar detection limits. This design exemplifies the superiority of tFNA-based interface engineering for nucleic acid diagnostics. Building on the universality of the tFNA platform, Lin *et al.* further demonstrated in another study that tFNAs could be flexibly modified with different aptamers or recognition elements to detect various analytes-ranging from nucleic acids to whole cells [108]. The tFNA-based system demonstrated ultrasensitive detection limits down to 10 attomolar (amol/L) for miRNAs and 1 pg/mL for prostate-specific antigen (PSA) in clinical serum samples-performance that rivals or exceeds traditional polymerase chain reaction (PCR) and enzyme-linked immunosorbent assay (ELISA) assays. The authors also successfully expanded its application to circulating tumor cell detection by taking advantages of multivalent aptamer interactions for cell capture and signal amplification *via* a hybridization chain reaction (HCR) strategy. This work exemplifies how tFNAs can bridge molecular diagnostics and point-of-care electrochemical sensing. The platform ensures reproducibility and high-density functionalization and serves as a modular framework adaptable to diverse sensing needs. Similarly, Liang *et al.* developed an innovative electrochemical biosensor for the ultrasensitive detection of microRNA-155, a key biomarker implicated in various cancers and inflammatory conditions [109]. The major design involves a synergistic catalytic nanoprobe, constructed by anchoring a hairpin DNA substrate onto a tFNA scaffold. This structural organization enables precise spatial positioning and stability of the functional elements, significantly enhancing the hybridization efficiency and reaction kinetics. Upon recognition of the target miRNA, the system triggers an improved cascade strand displacement reaction (CSDR) that intensifies the signal without the need for enzymatic assistance. The tFNA structure plays a role in facilitating efficient initiation of the CSDR and minimizing background noise by spatially isolating reactive components until the specific target is introduced. This combination of tFNA-based architecture and non-enzymatic signal amplification resulted in an exceptionally low limit of detection of 0.22 fmol/L for miRNA-155, making it suitable for early-stage disease diagnosis. Moreover, the platform demonstrated high specificity, stability in serum samples, and potential for point-of-care applications, underscoring the value of tFNAs in constructing next-generation biosensors for nucleic acid targets. A recent study by Zhang *et al.* introduced an advanced hybrid biosensor design that integrated tFNAs with catalytic hairpin assembly (CHA) for the detection of carcinoembryonic antigen (CEA) [110]. Here, tFNAs provided a stable and spatially optimized anchoring site for aptamers, while CHA served as an amplification mechanism to enhance electrochemical signals. The synergy between tFNAs and CHA enabled highly sensitive and specific cancer biomarker detection, which holds promise for early diagnostics.

The integration of tFNAs into CRISPR-based biosensors has opened new possibilities for nucleic acid detection by improving enzyme-substrate proximity, signal amplification, and modularity of the sensing system. These platforms capitalize on the trans-cleavage activity of CRISPR effector proteins (*e.g.*, Cas12a, Cas13a), with tFNAs acting as scaffolds to present DNA reporters or amplify recognition elements. As shown in Fig. S5 (Supporting information), Li *et al.* reported Framework-Hotspot reporters (FHRs) with different local densities to investigate their effect on trans-cleavage activity of Cas12a (Fig. S5a) [111]. They first designed and synthesized tetrahedral DNA framework (no reporter, named FHR0) and tetrahedral DNA framework-based FHRs at four different reporter densities (named FHR1, FHR2, FHR3 and FHR4, respectively) (Fig. S5b). The AFM and TEM results confirmed that the FHR4 present tetrahedral shape (Fig. S5c). They further extend the application for the detection of non-nucleic acid targets (Fig. S5d). Such modular platform could accurately identify prostate-specific antigen in patient samples and performed good correlation with clinical diagnosis. Another innovative example is the use of tFNAs in Cas13a-mediated detection. In the study by Li *et al.*, tFNAs were utilized to precisely organize recognition probes and improve signal amplification for detecting rare circulating tumor cells (CTCs) [112]. The tFNA scaffolds played a crucial role in enhancing the sensitivity and reliability of this biosensor. Their precise nanoscale geometry enabled optimal presentation of capture probes, ensuring effective target cell recognition even in complex biological fluids such as blood. Once the CTCs were captured *via* aptamer-functionalized tFNAs, the system leveraged Cas13a's collateral cleavage activity, which is activated upon target RNA recognition. This process initiated a cascade of cleavage events on fluorescent or electrochemical reporter RNAs, generating a robust and quantifiable signal. The combined use of CRISPR/Cas13a and tFNAs thus further increases detection sensitivity while ensuring biocompatibil-

ity and modularity, making it suitable for clinical liquid biopsy applications.

One pioneering example in the field of bioimaging is provided by Xu *et al.*, who proposed a multimodal serial multivariate signal amplification strategy based on framework nucleic acid for simultaneous absolute quantification of three different miRNAs in a single cell [113]. The detection sensitivity of the three miRNAs increased by six orders of magnitude at the same time, meeting the requirements for quantification of trace miRNAs in a single cell.

In the field of applying tFNAs in intracellular molecular sensing, Zhu *et al.* took advantage of the biocompatibility and capacity for spatially resolved functionalization of tFNAs and designed a triplex-functionalized DNA tetrahedral nanoprobe for the dual detection of intracellular pH and tumor-associated mRNA biomarkers [114]. This nanostructure incorporated a pH-responsive i-motif and a fluorophore-quencher pair, along with a hairpin probe specific to survivin mRNA. Utilizing triplex-forming sequences and a HCR mechanism, the nanoprobes exhibited amplified fluorescence signals in response to acidic environments and target mRNA presence. The modularity of the tFNA also allowed these sensing elements to be arranged with nanometer precision, enabling simultaneous, real-time monitoring of intracellular pH fluctuations and mRNA expression in live tumor cells. The dual-readout system provided spatially and temporally resolved signals with high sensitivity and specificity, demonstrating strong potential for early cancer diagnostics and monitoring tumor microenvironmental changes.

Further expanding the use of tFNAs in protein imaging, Ding *et al.* introduced a quantitative single-molecule detection (SMD) system based on DNA tetrahedron fluorescent nanolabels [115]. In this design, they constructed fluorescent nanolabels by intercalating SYBR Green I into DNA tetrahedron nanostructures, which were then conjugated to streptavidin-antihuman IgG antibodies. These complexes bound to human IgG immobilized on silanized glass substrates. Using epi–fluorescence microscopy and electron multiplying chargecoupled device (EMCCD) imaging, the researchers counted fluorescent spots corresponding to single protein molecules. The tFNA-enhanced SMD method enabled precise quantification of protein expression at the single-molecule level and in complex biological matrices, indicating promising applications in ultrasensitive clinical diagnostics.

Multiplexed imaging of intracellular microRNAs has also been realized using tFNA frameworks. Zhu *et al.* developed a DNA nanostructure encoding three miRNA-specific probes into distinct tetrahedral vertices, enabling simultaneous visualization of miR-21, miR-122, and miR-155 entering living cells without transfection agents [116]. Upon binding to their specific miRNA targets, the TDFs formed active DNAzyme structures, initiating a catalytic reaction that led to circular fluorescence signal amplification. The encoded tFNA achieved high spatial resolution, minimized cross-reactivity, and allowed real-time, multiplexed detection in single cells. Fluorescence signal amplification was accomplished *via* CHA, enhancing detection sensitivity while maintaining structural integrity and cellular uptake efficiency. This platform demonstrated the utility of tFNAs in profiling multiple gene expression targets within heterogeneous cellular environments.

To enhance the imaging of tumor cells *in vitro*, He *et al.* developed a biocompatible and targeted magnetic resonance imaging (MRI) contrast agent by integrating gadolinium-doped nanohydroxyapatite (Gd-HAp) with tFNAs conjugated with the AS1411 aptamer [117]. The AS1411 aptamer specifically binds to nucleolin, a protein overexpressed on tumor cell membranes, facilitating targeted imaging. After application, the resulting hybrid nanostructures exhibited enhanced colloidal stability and cellular internalization efficiency, enabling improved T1-weighted contrast *in vitro*. This approach integrates the biocompatibility of hydroxyapatite, the specificity of aptamer targeting, and the structural advantages of DNA nanotechnology to improve tumor cell imaging.

Further illustrating the multifunctional potential of tFNA-based nanodevices, He *et al.* developed a smart, all-in-one DNA nanostructure capable of simultaneously performing ratiometric dual-spectral fluorescence imaging of intracellular microRNAs and executing multimodal synergistic cancer therapy [118]. This nanodevice was constructed by integrating a tetrahedral DNA framework with up-conversion nanoparticles and gold nanorods, enabling precise intracellular delivery, controlled signal readout, and efficient photothermal and photodynamic therapeutic responses. The tFNA scaffold served as a programmable carrier for dual-emission fluorophores, allowing for highly specific and quantitative ratiometric imaging of miR-21, a tumor-associated microRNA. Upon illumination, the nanodevice has enabled accurate molecular diagnostics through dual-spectral fluorescence and triggered localized thermal and reactive oxygen species generation, thus achieving targeted cancer cell ablation. This integrated platform highlights the versatility of tFNAs in combining diagnostic imaging with therapy-realizing true theranostic capabilities within a single nanostructure-and underscores their value in precision oncology applications.

3.2. Edge-functionalized loading

The structural basis for the "horn attack" internalization mechanism of tFNAs lies in their four vertices. However, attaching programmed functionalities directly to these vertices often increases the overall size of the nanostructure and hampers efficient cellular uptake and tissue penetration. In contrast, when functional nucleic acid sequences are integrated into the eighth nucleotide of the tFNA side strand (counting from the 5′ to 3′ direction, with the unpaired vertex nucleotide designated as position zero), these sequences are encapsulated within the internal cavity of the tFNA. This configuration preserves both the structural integrity and size of the tFNA while enhancing the stability of the loaded nucleic acids. Moreover, loading targeting aptamers at the 13^{th} nucleotide of the side strand positions them on the exterior of the tFNA structure, thereby allowing effective target recognition and binding [119–122].

Traditional tFNA-based microRNA delivery strategies often involve the direct conjugation of therapeutic nucleic acids to the vertices or arms of the tFNA. However, the external exposure of these miR molecules renders them susceptible to degradation, compromising their therapeutic efficacy. To overcome this limitation, functional nucleic acid sequences can be inserted into the edges of tFNAs. For example, Li *et al.* developed a bioswitchable miR delivery system (BiRDS) by replacing the peripheral edges of tFNAs with miR functional sequences. This design retains the native tetrahedral topology while significantly enhancing the nucleic acid loading capacity. More importantly, it markedly improves the stability of the miR cargo under physiological conditions [45].

In addition, the double-helical structure of DNA provides multiple binding modes for small-molecule drugs. Through groove intercalation, these compounds can intercalate into the grooves between the two strands, allowing for stable incorporation. Positively charged peptides and proteins can associate with the negatively charged phosphate backbone of tFNAs *via* electrostatic interactions. Furthermore, hydrogen bonding has also been implicated as a key contributor to the binding affinity between small molecules and tFNA [65].

3.2.1. Drug delivery

In a recent study, miRNA-124 was efficiently loaded onto edges of tFNAs, positioned within the internal structure of the tetra-

hedron, thereby enhancing its stability and cellular delivery. The tFNA-based platform demonstrated significant improvements in miRNA loading capacity and therapeutic efficacy. The side-chain modification not only ensured stable encapsulation but also facilitated targeted delivery of miRNA-124 to ischemic brain regions. This delivery system leveraged the inherent structural advantages of tFNA, allowing for controlled release of miRNA-124, ensuring precise therapeutic outcomes while minimizing off-target effects. The successful use of miRNA-124 in tFNA nanocarriers further highlights the potential of tFNAs in gene therapy, particularly in treating neurological conditions such as acute ischemic stroke [120].

As shown in Fig. S6 (Supporting information), Li *et al.* were inspired by the Chinese cultural heritage symbol "Sun God Bird" and designed a bioswitchable miR inhibitor delivery system (BiRDS) (Fig. S6a), which consists of three miR inhibitors (the three immortal birds) and a nucleic acid core (the central sun) (Fig. S6b) [45]. Compared to traditional delivery systems, BiRDS maintains the 3D configuration of tFNA and exhibits strong cellular entry ability (Fig. S6c). Moreover, the small size of this structure gives it strong tissue permeability. BiRDS provides sufficient protection for the transported miRNA and exhibits excellent stability under high enzyme or serum conditions (Fig. S6d). As shown in Figs. S6e and f, BiRDS exhibited a strong fluorescence signal after 24 h of drug penetration. The BiRDS also exhibited the most excellent therapeutic effect for treatment of skin aging (Fig. S6g).

3.2.2. Tissue engineering and regenerative medicine

As shown in Fig. S7 (Supporting information), Li *et al.* developed a 3D hybrid scaffold loaded with tfNAs and clindamycin (CLI), a common antibiotic used to treat osteomyelitis, named TDN–CLI using bioprinting technology (Fig. S7a) [65]. The successful synthesis of TDN–CLI was verified by PAGE (Fig. S7b), TEM (Fig. S7c), AFM (Fig. S7d), and Zeta potentials (Fig. S7e). According to infected bone defect model in SD rats, the TDN–CLI loaded scaffold showed excellent osteogenic and antibacterial properties (Fig. S7f).

As shown in Fig. S8 (Supporting information), Xie *et al.* developed a transdermal system for local treatment of skin photodamage, consisting of tFNAs and lipoic acid (LA) called TLA (Fig. S8a) [123]. The PAGE (Fig. S8b) and HPCE (Fig. S8c) results confirmed the successful synthesis of tFNAs and the successful binding of tFNAs and LA, with no significant by-products. After experiencing photodamage modeling and transdermal drug delivery treatment, the skin conditions were recorded (Fig. S8d). The TLA group showed significant improvement in skin erythema and rapid healing of skin injuries (Fig. S8e). Fluorescence staining confirmed that tFNA and TLA are mainly distributed in hair follicles and skin appendages (Fig. S8f).

3.2.3. Biosensing and bioimaging

In a separate study (Fig. S9 in Supporting information), Liu *et al.* designed a DNA framework nanomachine (DFN) based on tFNA, which can autonomously respond to pH changes within a single synaptic vesicle and change shape, and display adaptive fluorescence color through mechanical fluorescence activation mechanism (Fig. S9a) [124]. This nanomachine can target cholesterol groups on the vesicle membrane for labeling, and after internalization, it can be trapped alone in a single endocytic vesicle of synaptic cells (Fig. S9b). According to the confocal laser scanning microscope (CLSM) results, the DFNs can undergo endocytosis and exocytosis procedures through vesicle circulation (Figs. S9c and d). The design of this nanomachine not only improves the signal-to-noise ratio of fluorescence color change but also provides a new technological means for studying neurotransmitter release and neural signal transduction.

3.3. Internal encapsulation

The edges of tFNAs are formed by rigid double-helical DNA, which defines a central cavity capable of carrying nanoparticles. This rigidity provides structural stability and allows the cavity to function as a controllable "cage" to release "cargo" in response to specific cellular or environmental stimuli. Besides, targeted modifications on tFNAs further enable precise delivery to specific sites. Moreover, tFNAs can be rapidly and efficiently assembled through self-assembly, making them attractive carriers for molecular encapsulation and delivery [48,125,126].

3.3.1. Drug delivery

Gao *et al*. developed a tFNA nanobox carrier for target siRNA, embedding the siRNA *via* complementary pairing at both ends. This strategy leverages the inherent stability of tFNA to protect the siRNA (Fig. S10a) [48]. Building on this protective delivery, a pH-responsive release mechanism was introduced by incorporating a C-rich sequence, forming an i-motif structure. This enables the carrier to disassemble or change conformation in the hydrogen-ion-rich (acidic) environment of lysosomes following cellular internalization, allowing for controllable release of the target siRNA (Fig. S10b). Live-cell imaging (Fig. S10c) revealed rapid cellular uptake; Cy5-labeled siRNA was detected in macrophages within 10 min of incubation with nanobox-siR. Crucially, the observed spatial separation between Cy3 (carrier) and Cy5 (siRNA) signals, with an excess of Cy5 signal relative to Cy3 (white arrows show overlap, red arrows show individual Cy5 signals), provides evidence that the i-motif structure responded to the acidic lysosomal pH, triggering siRNA release. The biological efficacy was subsequently assessed (Fig. S10d). qPCR analysis (Fig. S10e) confirmed that the nanobox-siR resulted in a significant reduction in TNFα mRNA expression.

As shown in Fig. S11 (Supporting information), Wu *et al*. developed a multifunctional DNA tetrahedron-based nanoplatform for efficient bacterial elimination (Fig. S11a). AFM images showed the successful assembly of ciprofloxacin- and AgNP-loaded DNA tetrahedrons, with the silver nanoparticles encapsulated within the inner cavity of the tetrahedral structure, and an average diameter of ~16 nm (Fig. S11b). *In vitro* antibacterial experiments demonstrated that these targeted delivery systems significantly increased antibiotic accumulation in *Escherichia coli* and induced efficient bacterial killing, as shown by confocal imaging and live/dead staining (Fig. S11c). Furthermore, *in vivo* studies using infected wound models in mice revealed that treatment with the dual-antibiotic-loaded DNA tetrahedron accelerated wound healing (Fig. S11d). These results indicate the strong potential of DNA tetrahedron-based nanocarriers for targeted anti-infection therapy [125].

3.3.2. Biosensing and bioimaging

The incorporated fluorescent DNA framework (FDF)-based systems have been investigated for their potential in ultrahigh-sensitivity cancer imaging and image-guided surgery. As shown in Fig. S12 (Supporting information), Liu *et al*. designed size- and shape-resolved FDF dots by non-covalently encapsulating a newly synthesized hydrophobic near-infrared-Ib (NIR-Ib) dye (Sq964) within tetrahedral DNA nanostructures to achieve near-single-cell-level tumor imaging (Fig. S12a). AFM images confirmed the successful assembly of these tetrahedral frameworks with mean sizes of ~8.5 nm (Fig. S12b). Long-term imaging showed stable tumor signals over 11 days without attenuation, facilitating precise monitoring of tumor progression (Fig. S12c). Moreover, upon intravenous administration of FDF-dot-labeled 4T1 breast cancer cells into nude mice, the *in vivo* NIR-II fluorescence imaging revealed clear visualization of tumor cells down to ~40 cells, with significantly enhanced signal-to-background ratios (Fig. S12d) [126].

Table 1
Comparison of modification strategies for tFNAs.

Modification strategy	Loading capacity	Stability	Biocompatibility
Vertex Modification	Relatively low, limited by spatial constraints	High structural stability, but functionalization may impact stability	High biocompatibility, suitable for various *in vivo* applications
Edge-functionalized loading	Higher loading capacity, can accommodate larger molecules or multiple functional groups	Stable structure, but larger size may hinder cellular uptake and tissue penetration	High stability of loaded molecules, suitable for gene and small molecule delivery
Internal encapsulation	Limited by the confined interior space	Excellent protection for sensitive cargo, such as siRNA or proteins	High biocompatibility, suitable for long-term *in vivo* use
Surface coating	Does not significantly affect loading capacity	Improves stability, reduces immune response, and enhances targeting ability	Biocompatibility enhanced through biomimetic coatings or targeting ligands

3.4. Surface coating

Although tFNAs possess excellent drug delivery capabilities, certain improvements are necessary to overcome their current limitations in practical applications: (1) Achieving unprompted endocytosis, (2) reducing immune activation and rapid blood clearance, and (3) enhancing targeting ability and stealth properties. In addition to modifying the framework structure, surface coating of tFNAs is another effective modification strategy. According to the properties of different outer membranes (such as extracellular vesicles, liposomes, red blood cell membranes), the stability of nanomaterials can be enhanced and the targeting can be improved, further expanding the application of tFNAs in biomedicine [127–129].

The engineered TTob@NPM nanocarrier has demonstrated remarkable antibacterial and immunomodulatory performance [127]. As shown in Fig. S13 (Supporting information), Zhang *et al.* constructed a bioinspired neutrophil-platelet hybrid membrane-coated tFNAs nanocarrier loaded with tobramycin (TTob@NPM) for the treatment of Pseudomonas aeruginosa infections (Fig. S13a). Transmission electron microscopy (TEM) revealed the successful assembly of the TTob complex with a characteristic core–shell structure after coating with the hybrid membrane (Fig. S13b). To evaluate its chemotactic targeting ability, TTob@NPM was subjected to μ-slide chemotaxis assays, which showed significantly enhanced migration toward higher bacterial gradients (Fig. S13c). In mouse models of acute *P. aeruginosa* lung infection, intranasal administration of TTob@NPM resulted in the lowest bacterial burden among treatment groups (Fig. S13d). Immunofluorescence staining further demonstrated increased M1-like macrophage polarization and reduced MDSCs recruitment in lung tissues, suggesting effective reversal of the immunosuppressive microenvironment (Fig. S13e). Collectively, these results highlight the potential of TTob@NPM as a multifunctional therapeutic platform integrating targeted antibiotic delivery, toxin neutralization, and immunomodulation for treating refractory bacterial infections.

As shown in Fig. S14 (Supporting information), Cui *et al.* developed an exosome-like nanovesicle system encapsulating antimicrobial peptide-modified tFNAs (Exo@tac) for oral treatment of Parkinson' s disease (Fig. S14a) [128]. TEM and AFM confirmed the successful assembly of Exo@tac with a stable morphology and an average diameter of ∼150 nm (Fig. S14b). *In vitro* experiments demonstrated that Exo@tac effectively targeted *E. coli*, resulting in significant bacterial membrane damage and reduced viability, as evidenced by scanning electron microscope (SEM) and viability assays (Fig. S14c). Furthermore, *in vivo* administration of Exo@tac in PD mouse models significantly improved motor symptoms and enhanced striatal dopamine-related markers (Fig. S14d). These results highlight the potential of Exo@tac as an oral nanoplatform for targeted gut microbiota modulation and neuroprotection.

To achieve safe and precise chemotherapeutic delivery, Ma *et al.* designed a biomimetic, pH-responsive nanoplatform by conjugating the cytotoxic agent maytansine (DM1) to a human epidermal growth factor receptor 2 (HER2)-targeting DNA tetrahedron (HApt-tFNA@DM1, HTD) and embedding it within a hybrid vesicle composed of erythrocyte membranes and synthetic liposomes [129]. As shown in Fig. S15 (Supporting information), the biomimetic coating improved systemic circulation and enabled pH-triggered release within the tumor microenvironment (Fig. S15a). Confocal imaging demonstrated preferential uptake of Cy5-labeled HTD by HER2-positive tumor cells, along with significant microtubule disruption, indicating effective intracellular drug release (Fig. S15b). *In vivo* studies in a xenograft model showed enhanced tumor accumulation and potent tumor growth inhibition with minimal off-target toxicity (Fig. S15c). This work highlights the potential of combining DNA nanostructures with cell-mimicking vesicles for targeted, stimuli-responsive cancer therapy.

4. Advantages of tFNAs over conventional nanomaterials

As shown in Table 1, functionalized tFNAs in various forms significantly enhance performance by modulating their structure and properties, playing a crucial role in drug delivery, tissue engineering and regenerative medicine, as well as biosensing and bioimaging. Compared to traditional nanocarriers such as liposomes, dendrimers, polymeric nanoparticles, and viral vectors, tFNAs exhibit distinct advantages rooted in their precise structural programmability, biocompatibility, and functional versatility [130–133]. Their uniform size distribution and rigid DNA-based architecture confer high structural stability, predictable pharmacokinetics, and enhanced cellular uptake [134–136]. The negatively charged, hydrophilic surface reduces nonspecific protein adsorption and prolongs circulation time [137,138], while their modular design enables facile site-specific functionalization with aptamers, antibodies, or small molecules *via* complementary base pairing [128,139]. Moreover, tFNAs provide superior nucleic acid payload protection and controlled release mechanisms, such as pH-responsive unfolding or enzyme-triggered disassembly, tailored for intracellular delivery [78,140]. Unlike viral systems, which carry risks of insertional mutagenesis, immunogenicity, and limited cargo capacity [141,142], tFNAs are non-immunogenic, chemically synthesized, and can carry diverse functional modules, including DNA, RNA, proteins, and small molecules [143,144]. Their capacity to encapsulate Cas9 ribonucleoprotein complexes or guide RNAs further enhances genome editing efficiency while mitigating off-target effects and immunogenicity [112]. In imaging applications, tFNAs outperform conventional organic dyes and quantum dots by combining excellent biocompatibility and biodegradability with programmable architectures that support precise spatial arrangement and high-density loading of imaging agents, thereby amplifying signal inten-

sity and improving targeting specificity [26,28,29,145–147]. Collectively, these advantages position tFNAs as a next-generation multifunctional platform with broad potential across drug delivery, tissue engineering, regenerative therapy, biosensing, and diagnostic imaging [148–150].

5. Challenges and optimization directions

While substantial progress has been made in the field of tFNAs, to unleash their full potential for biomedical applications requires overcoming several key challenges. (1) *In vivo* stability: the inherent susceptibility of DNA to degradation by nucleases in physiological environments calls for strategies to enhance the stability, such as the incorporation of modified nucleotides or protective coatings to prevent degradation in the bloodstream [151–156]. (2) Manufacturing scalability: the development of efficient and cost-effective methods for large-scale production is crucial for the widespread adoption of tFNAs [157–162]. Recent studies have focused on improving the scalability of tFNA synthesis. For instance, Li *et al.* demonstrated that optimizing the self-assembly process and stabilizing reaction conditions can enhance batch consistency, which is essential for ensuring uniform quality in large-scale production [45]. However, further research is needed to refine these techniques and reduce production costs to meet the demands of clinical applications. (3) Clinical translation: translating these nanostructures into clinical use also demands rigorous preclinical testing and navigation of complex regulatory approval pathways. (4) Biocompatibility: careful consideration of the potential toxicity and immunogenicity of tFNAs is paramount, which requires thorough investigation into the effects of nanoscale structures and introduced chemical modifications, despite the generally biocompatible nature of DNA [163–167]. (5) Targeting capability: the targeting precision of tFNAs requires further refinement to minimize off-target effects through optimized controlled release mechanisms, and a more comprehensive understanding of biological system complexities is crucial for effectively navigating inherent pathways and molecular mechanisms, thereby enabling the successful development and implementation of DNA-based nanotherapeutics [168–173]. Additionally, strategies to improve tissue penetration and cellular uptake have been explored by modifying the surface properties of tFNAs with targeting ligands and biomimetic coatings. For example, Zhang *et al.* demonstrated that coating tFNAs with neutrophil-mimicking membranes significantly improved their cellular uptake and targeting efficiency in inflammatory tissues [127]. Optimizing these aspects will facilitate the development of tFNAs into a versatile nanoplatform for theranostic applications.

6. Conclusions and prospects

In summary, this review has comprehensively explored the field of engineered tFNAs. We have traced their development from rational design and precision fabrication to versatile functionalization strategies, emphasizing how their unique structure-function relationships underpin their remarkable programmable biofunctionalities. Moving beyond conventional drug delivery, we highlighted their significant potential and recent advancements across diverse biomedical applications, including tissue engineering, biosensing and bioimaging, and particularly their emerging role in translational theranostics. While considerable progress has been made, realizing the full potential of tFNAs in clinical settings necessitates overcoming key challenges related to manufacturing scalability, pharmacokinetic optimization, and regulatory approval. Continued research focusing on innovative design principles, enhanced *in vivo* performance, and addressing these translational hurdles is crucial. Ultimately, engineered tFNAs stand as a powerful and adaptable platform, poised to drive advancements in personalized nanomedicine and next-generation therapeutic and diagnostic strategies, with the potential to significantly impact human health.

Future research directions should focus on several key areas to further advance the field of tFNAs. This includes developing biodegradable DNA analogs or polymers to encapsulate or support tFNAs, further enhancing their biocompatibility and minimizing long-term accumulation within the body [174–178]. Integrating machine learning and AI-based methodologies for faster and more precise design of novel tFNAs is also crucial [179–182]. Furthermore, exploring combined therapies that integrate drug delivery, gene therapy, and diagnostic capabilities within a single DNA tetrahedron holds promise for developing more effective multimodal therapeutic strategies [183–188]. Continued innovation in advanced characterization techniques is needed to evaluate the structural properties and functional performance of tFNAs under complex biological conditions [189–192]. Finally, expanding the application of tFNAs to new therapeutic areas through the development of novel delivery strategies and the incorporation of emerging therapeutic modalities remains an ongoing and important area of focus [193–200]. Particularly, integration of artificial intelligence (AI) in tFNAs design is one of the most pressing areas for future research. AI-driven approaches, such as machine learning and deep learning algorithms, hold significant promise for optimizing tFNA structures, predicting their interactions with biological targets, and enhancing their efficiency in clinical applications. For example, AI can be employed to accelerate the design of tFNAs with improved biocompatibility and drug delivery properties, as well as to identify optimal functionalization strategies for targeted therapies [200,201].

CRediT authorship contribution statement

Tingting Zuo: Data curation, Conceptualization. **Tao He:** Data curation, Conceptualization. **Yuan Gao:** Data curation. **Siyi Yang:** Data curation. **Yun Wang:** Writing – review & editing. **Zhengyang Yang:** Formal analysis. **Chao Zhang:** Conceptualization. **Yunfeng Lin:** Writing – review & editing, Funding acquisition, Conceptualization.

Declaration of competing interest

The authors declare that they have no known competing financial interests or personal relationships that could have appeared to influence the work reported in this paper.

Acknowledgments

This work was financially supported by the National Natural Science Foundation of China (Nos. 82373393, 82202884, 22304072, 82370929), Xinjiang Uygur Autonomous Region "Tianchi Yingcai" Project (No. 2023TCYCQNBS02), Xinjiang Uygur Autonomous Region Colleges and Universities Basic Research Operating Expenses Scientific Research Project (No. XJEDU2022P106), the Training Fund for Open Projects at Clinical Institutes and Departments of Capital Medical University (No. CCMU2022ZKYXY008), Sichuan Science and Technology Program (No. 2022NSFSC0002), Sichuan Province Youth Science and Technology Innovation Team (No. 2022JDTD0021), and Research and Develop Program, West China Hospital of Stomatology Sichuan University (Nos. RD03202302, RCDWJS2024–1).

Supplementary materials

Supplementary material associated with this article can be found, in the online version, at doi:10.1016/j.cclet.2025.112102.

References

[1] F. Han, S. Gu, A. Klimas, et al., Science 378 (2022) 1325.
[2] D.A. Leigh, Nature 638 (2025) 38.
[3] B. Crew, Nature 609 (2022) S1.
[4] A. Javaid, S. Hameed, L. Li, et al., Funct. Integr. Genomics. 24 (2024) 216.
[5] V.K. Chaturvedi, A. Singh, V.K. Singh, M.P. Singh, Curr. Drug Metab. 20 (2019) 416.
[6] T. Tian, Y. Li, Y. Lin, Bone Res. 10 (2022) 40.
[7] C. Zhang, X. Jing, L. Guo, et al., Nano Lett. 21 (2021) 5834.
[8] M. DeLuca, S. Sensale, P.A. Lin, G. Arya, ACS Appl. Bio Mater. 7 (2024) 626.
[9] C. Zhang, Y. Yuan, K. Wu, et al., Nano Lett. 22 (2022) 468.
[10] L. Shen, P. Wang, Y. Ke, Adv. Healthc. Mater. 10 (2021) e2002205.
[11] S. Nummelin, B. Shen, P. Piskunen, et al., ACS Synth. Biol. 9 (2020) 1923.
[12] J. Liu, L. Yan, S. He, J. Hu, Nano Res. 15 (2022) 3504.
[13] Z. He, K. Shi, J. Li, J. Chao, iScience 26 (2023) 106638.
[14] S. Vecchioni, R. Lo, Q. Huang, et al., Small 21 (2025) e2407604.
[15] F. Deng, Y. Li, B. Yang, et al., Nat. Commun. 15 (2024) 1818.
[16] Q. Chen, Y. Liu, Q. Chen, et al., Small 20 (2024) e2405231.
[17] A. Rodriguez, D. Gandavadi, J. Mathivanan, et al., Small 19 (2023) e2300040.
[18] S. Li, T. Tian, T. Zhang, Y. Lin, X. Cai, Nat. Protoc. 20 (2025) 336.
[19] T. Zhang, T. Tian, R. Zhou, et al., Nat. Protoc. 15 (2020) 2728.
[20] J. Gu, J. Liang, T. Tian, Y. Lin, JACS Au 5 (2025) 486–520.
[21] Y. Zhang, Y. Sun, H. Liao, S. Shi, Nanoscale 17 (2025) 4974–4999.
[22] Z. Yang, L. Shi, Y. Wang, et al., Small 21 (2025) e2410162.
[23] Q. Fan, B. Sun, J. Chao, Small. Methods 9 (2025) e2401360.
[24] L. Liang, J. Li, Q. Huang, et al., Angew. Chem. Int. Ed. 53 (2014) 7745–7750.
[25] X. Li, L. Li, X. Fu, et al., Cell Prolif. 58 (2025) e13736.
[26] R. Wang, Y. Liu, Y. Zhang, et al., J. Am. Chem. Soc. 147 (2024) 7545.
[27] Y.C. Ge, W.T. Cui, X.R. Shao, et al., ACS Appl. Mater. Interfaces 11 (2019) 27588–27597.
[28] Y. Li, S. Wang, Y. Dong, et al., Adv. Healthc. Mater. 13 (2024) e2304381.
[29] L. Tan, J. Xie, C. Liao, et al., J. Nanobiotechnol. 22 (2024) 682.
[30] L. Wang, Q. Yao, X. Guo, et al., J. Nanobiotechnol. 22 (2024) 392.
[31] Y. Zhu, R. Shi, W. Lu, S. Shi, Y. Chen, Nanoscale 16 (2024) 7363.
[32] T. Zhang, T. Tian, Y. Lin, Adv. Mater. 34 (2022) e2107820.
[33] X. Chen, Z. Xu, Y. Gao, et al., Adv. Mater. 36 (2024) e2406118.
[34] T. Tian, T. Zhang, S. Shi, et al., Nat. Protoc. 18 (2023) 1028–1055.
[35] T. Zhang, X. Zhang, S. Shi, Y. Lin, Adv. Funct. Mater. 33 (2023) 2213401.
[36] J. Li, R. Yan, S. Shi, Y. Lin, Expert. Opin. Drug Deliv. 20 (2023) 1511–1530.
[37] J. Liu, H. Cabral, P. Mi, Adv. Drug Deliv. Rev. 207 (2024) 115239.
[38] Y. Zheng, S. Luo, M. Xu, et al., Acta Pharm. Sin. B 14 (2024) 3876–3900.
[39] Z. Cheng, H. Que, L. Chen, Q. Sun, X. Wei, Pharmaceutics 14 (2022) 1372.
[40] Y. Wei, X. Xia, H. Li, H. Gao, Expert. Opin. Drug Deliv. 20 (2023) 1713–1730.
[41] Y. Yao, M. Yang, S. Shi, Curr. Drug Metab. 24 (2023) 338–352.
[42] J. Huang, K. Xiao, Pharmaceutics 14 (2022) 1586.
[43] X. Li, Y. Lan, X. Fu, et al., Aggregate 5 (2024) e603.
[44] Y. Chen, X. Chen, B. Zhang, et al., Signal. Transduct. Target. Ther. 9 (2024) 28.
[45] S. Li, Y. Liu, T. Zhang, et al., Adv. Mater. 34 (2022) e2204287.
[46] W. Wang, M. Lin, W. Wang, Z. Shen, Z.S. Wu, Bioact. Mater. 33 (2024) 279–310.
[47] X. Zhang, N. Liu, M. Zhou, S. Li, X. Cai, Curr. Stem Cell Res. Ther. 16 (2021) 48.
[48] Y. Gao, X. Chen, T. Tian, et al., Adv. Mater. 34 (2022) e2201731.
[49] Y. Li, J. Li, Y. Chang, et al., Chem. Eng. J. 496 (2024) 153723.
[50] J. Xu, G.A. Wang, L. Gao, et al., Nat. Commun. 14 (2023) 4248.
[51] A.A. Almaqwashi, T. Paramanathan, I. Rouzina, M.C. Williams, Nucleic Acids Res. 44 (2016) 3971.
[52] K.T. McQuaid, A. Pipier, C.J. Cardin, D. Monchaud, Nucleic Acids Res. 50 (2022) 12636.
[53] B. Zhang, T. Tian, D. Xiao, Adv. Funct. Mater. 32 (2022) 2109728.
[54] W. Yuan, M. Huang, W. Chen, et al., J. Nanobiotechnol. 22 (2024) 700.
[55] R. Chen, D. Wen, W. Fu, et al., Cell Prolif. 55 (2022) e13206.
[56] X. Zhou, Y. Lai, X. Xu, et al., Cell Prolif. 56 (2023) e13407.
[57] Y. Chen, S. Shi, B. Li, et al., ACS Appl. Mater. Interfaces 14 (2022) 13136–13146.
[58] Q. Wang, J. Cheng, F. Liu, et al., Adv. Sci. 11 (2024) e2306622.
[59] J. Li, Y. Yao, Y. Wang, et al., Adv. Mater. 34 (2022) e2202513.
[60] J.M. Weck, A. Heuer-Jungemann, Nat. Commun. 16 (2025) 1556.
[61] D. Mathur, E.R. Henderson, ACS Synth. Biol. 2 (2013) 180.
[62] F. Liu, X. Liu, W. Gao, et al., iScience 26 (2023) 106208.
[63] R. Shi, Y. Zhu, Y. Chen, Y. Lin, S. Shi, J. Control. Release 375 (2024) 155–177.
[64] Y. Li, Z. Cai, W. Ma, et al., Bone Res. 12 (2024) 14.
[65] J. Li, Y. Lai, M. Li, X. Chen, Chem. Eng. J. 435 (2022) 134855.
[66] R. Yan, W. Cui, W. Ma, et al., ACS Nano 17 (2023) 8767–8781.
[67] Y. Zhang, C. Mao, Y. Zhan, et al., ACS Appl. Mater. Interfaces 14 (2022) 39819-38829.
[68] T. Zhang, W. Cui, T. Tian, S. Shi, Y. Lin, ACS Appl. Mater. Interfaces 12 (2020) 47115–47126.
[69] S. Shi, Y. Li, T. Zhang, et al., ACS Appl. Mater. Interfaces 13 (2021) 57067–57074.
[70] L. Chen, J. Luo, J. Zhang, et al., Int. J. Mol. Sci. 24 (2023) 11575.
[71] H. Qian, T. Zhou, Y. Fu, et al., Mol. Ther. Nucleic Acids 27 (2022) 763–773.
[72] W. Ma, Y. Zhan, Y. Zhang, et al., ACS Appl. Mater. Interfaces 12 (2020) 2095–2106.
[73] Y. Lin, Q. Li, L. Wang, et al., Int. J. Oral Sci. 14 (2022) 51.
[74] M. Liu, L. Hao, D. Zhao, J. Li, Y. Lin, ACS Appl. Mater. Interfaces 14 (2022) 38506–38514.
[75] L. Wang, Y. Wang, T. Lu, et al., Adv. Funct. Mater. 34 (2024) 2310749.
[76] J. Li, L. Xiao, N. Yan, et al., Adv. Funct. Mater. 31 (2021) 2104141.
[77] Q. Li, D. Zhao, X. Shao, et al., ACS Appl. Mater. Interfaces 9 (2017) 36695–36701.
[78] Q. Fan, Z. Li, J. Yin, et al., Biomaterials 301 (2023) 122283.
[79] X. Qin, L. Xiao, N. Li, et al., Bioact. Mater. 14 (2022) 134–144.
[80] M. Zhang, X. Qin, Y. Gao, et al., Adv. Sci. 10 (2023) 2303706.
[81] M. Zhou, Y. Tang, Y. Lu, et al., ACS Nano 19 (2025) 3455–3469.
[82] X. Peng, S. Fang, B. Ji, et al., Nano Lett. 16 (2021) 6946–6951.
[83] J. Li, X. Mao, T. Zhao, et al., Angew. Chem. Int. Ed. 64 (2025) e202416988.
[84] X. Xu, Y. Fu, D. Luo, et al., Cell Prolif. 57 (2024) e13695.
[85] Y. Jin, X. Zhou, L. Chen, et al., ACS Nano 38 (2024) 26076–26087.
[86] W. Zhang, Y. Liu, Y. Luo, et al., Int. J. Biol. Macromol. 304 (2025) 140765.
[87] B. Chen, L. Mei, Y. Wang, G. Guo, Drug Discov. Today 26 (2021) 1018–1029.
[88] Z. Fang, L. Wan, L. Chu, Y. Zhang, J. Wu, Expert. Opin. Drug Deliv. 12 (2015) 1943–1953.
[89] P. Wu, J. Han, Y. Gong, et al., Pharmaceutics 14 (2022) 1990.
[90] S. Yang, H. Gao, Pharmacol. Res. 126 (2017) 97–108.
[91] Q. An, D. Wang, L. Huang, X. Chen, C. Wang, Front. Pharmacol. 15 (2024) 1498728.
[92] T. Tan, Q. Yang, D. Chen, et al., Asian J. Pharm. Sci. 16 (2021) 508–518.
[93] Y. Gao, K. Men, C. Pan, et al., Int. J. Nanomedicine 16 (2021) 5211–5232.
[94] L. Li, M. Yang, R. Li, et al., Anticancer Agents Med. Chem. 21 (2021) 910–918.
[95] W. Jia, R. Liu, Y. Wang, et al., Acta Pharm. Sin. B 12 (2022) 3354–3366.
[96] J. Gan, G. Du, C. He, et al., J. Control. Release 326 (2020) 297–309.
[97] J. Liang, B. Yang, X. Zhou, et al., Drug Deliv. 28 (2021) 272–284.
[98] Y. Li, Y. Gao, X. Zhang, H. Guo, H. Gao, Int. J. Pharm. 591 (2020) 119986.
[99] Y. Zhu, J. Xue, W. Chen, et al., J. Control. Release 322 (2020) 300–311.
[100] J. Li, M. Li, L. Tian, et al., Int. J. Pharm. 578 (2020) 119122.
[101] L. Wang, M.L. Javier, C. Luo, et al., Chin. Chem. Lett. 35 (2024) 109591.
[102] T. Tian, D. Xiao, T. Zhang, et al., Adv. Funct. Mater. 31 (2021) 2007342.
[103] D. Li, Z. Yang, Y. Luo, et al., Adv. Healthc. Mater. 11 (2022) e2101412.
[104] S. Li, Y. Liu, T. Tian, et al., Small 17 (2021) e2104359.
[105] D. Zhao, M. Liu, J. Li, et al., ACS Appl. Mater. Interfaces 13 (2021) 29439–29449.
[106] Y. Ge, Q. Wang, X. Qin, et al., ACS Appl. Mater. Interfaces 14 (2022) 19091–19103.
[107] M. Lin, J. Wang, G. Zhou, et al., Angew. Chem. Int. Ed. 54 (2015) 2151–2155.
[108] M. Lin, P. Song, G. Zhou, et al., Nat. Protoc. 11 (2016) 1244–1263.
[109] Z. Liang, D. Ou, D. Sun, et al., Biosens. Bioelectron. 146 (2019) 111744.
[110] K. Zhang, M. Pei, Y. Cheng, et al., J. Electroanal. Chem. 898 (2021) 115635.
[111] F. Li, J. Li, W. Yang, et al., Angew. Chem. Int. Ed. 62 (2023) e202305536.
[112] K. Li, S. Luo, S. Guan, et al., Talanta 247 (2022) 123531.
[113] C. Xu, S. Chen, S. Hu, et al., Anal. Chem. 95 (2023) 11061–11069.
[114] C. Zhu, J. Yang, J. Zheng, et al., Anal. Chem. 91 (2019) 15599–15607.
[115] Y. Ding, X. Liu, J. Zhu, L. Wang, W. Jiang, Talanta 125 (2014) 393–399.
[116] D. Zhu, Y. Wei, T. Sun, et al., Anal. Chem. 93 (2021) 2226–2234.
[117] Y. He, C. Lv, X. Hou, L. Wu, Anal. Chim. Acta 1138 (2020) 141–149.
[118] P. He, W. Han, C. Bi, et al., ACS Nano 15 (2021) 6961–6976.
[119] C.M. Erben, R.P. Goodman, A.J. Turberfield, Angew. Chem. Int. Ed. 45 (2006) 7414–7417.
[120] G.N. Du, Y.X. Yao, W. Chen, et al., ACS Appl. Mater. Interfaces 17 (2025) 11925–11936.
[121] X. Zhang, M. Zhang, M. Zhou, et al., ACS Appl. Mater. Interfaces 14 (2022) 6442–6452.
[122] Y. Ge, Q. Wang, Y. Yao, et al., Adv. Sci. 11 (2024) e2308701.
[123] Y. Xie, J. He, S. Li, et al., Adv. Funct. Mater. 33 (2023) 2303580.
[124] J. Liu, X. Jing, M. Liu, et al., Sci. Robot. 7 (2022) eabq5151.
[125] T. Wu, Y. Fu, S. Guo, et al., Aggregate 5 (2023) e402.
[126] X. Liu, B. Shi, Y. Gao, et al., Nat. Photonics. 19 (2024) 79–88.
[127] S. Zhang, T. Chen, W. Lu, et al., Adv. Sci. 12 (2025) e2411261.
[128] W. Cui, Z. Guo, X. Chen, et al., Sci. Bull. 69 (2024) 3925–3935.
[129] W. Ma, Y. Yang, J. Zhu, et al., Adv. Mater. 34 (2022) e2109609.
[130] J. Li, H. Pei, B. Zhu, et al., ACS Nano 11 (2011) 8783–8789.
[131] Y. Huang, W. Huang, L. Chan, B. Zhou, T. Chen, Biomaterials 103 (2016) 183–196.
[132] W. Ma, Y. Zhan, Y. Zhang, et al., Nano Lett. 19 (2019) 4505–4517.
[133] S. Shi, W. Fu, S. Lin, et al., Nanomedicine 21 (2019) 102061.
[134] T. Tan, J. Li, W. Fan, et al., Cell Prolif. 58 (2025) e13803.
[135] Z. Wang, H. Lu, T. Tang, et al., Cell Prolif. 55 (2022) e13316.
[136] C. Qi, Q. Sun, D. Xiao, et al., Int. J. Oral Sci. 16 (2024) 30.
[137] L. Wang, Y. Wang, Y. Jiang, et al., ACS Nano 17 (2023) 24187–24199.
[138] H. Pei, L. Liang, G. Yao, et al., Angew. Chem. Int. Ed. 36 (2012) 9020–9024.
[139] Y. Liu, Y. Sun, S. Li, et al., Nano Lett. 20 (2020) 3602–3610.
[140] Y. Zhang, W. Ma, Y. Zhu, et al., Nano Lett. 18 (2018) 5652–5659.
[141] M. Mietzsch, J. Hsi, A.R. Nelson, et al., Nat. Commun. 16 (2025) 3731.
[142] H. Costa-Verdera, V. Meneghini, Z. Fitzpatrick, et al., Nat. Commun. 16 (2025) 3694.
[143] M. Wei, S. Li, Z. Yang, et al., Nanomedicine 34 (2021) 102375.
[144] C. Dong, Y. Wang, Z. Chen, et al., Small 20 (2024) e2308562.
[145] N. Le, K. Kim, Int. J. Mol. Sci. 24 (2023) 12682.
[146] Z. Wang, B. Yao, Y. Xiao, X. Tian, Y. Wang, Chemosensors 11 (2023) 405.
[147] Y. Zhang, N. Cai, V. Chan, Biosensors 13 (2023) 311.

[148] D. Jiang, Y. Sun, J. Li, et al., ACS Appl. Mater. Interfaces 7 (2016) 4378–4384.
[149] Z. Liu, X. Chen, W. Ma, et al., Adv. Funct. Mater. 43 (2022) 2204587.
[150] Q. Zhang, S. Lin, S. Shi, et al., ACS Appl. Mater. Interfaces 4 (2018) 3421–3430.
[151] X. Shi, H. Chen, H. Yang, et al., ACS Appl. Mater. Interfaces 16 (2024) 50484.
[152] N. Ponnuswamy, M.M.C. Bastings, B. Nathwani, et al., Nat. Commun. 8 (2017) 15654.
[153] T. Zhang, M. Zhou, D. Xiao, et al., Adv. Sci. 9 (2022) e2202058.
[154] Y. Zhan, W. Ma, Y. Zhang, et al., ACS Appl. Mater. Interfaces 17 (2019) 15354–15365.
[155] F. Shen, Z. Xiong, Y. Wu, et al., Angew. Chem. Int. Ed. 62 (2023) e202301147.
[156] Y. Li, J. Li, S. Xu, et al., Adv. Healthc. Mater. 13 (2024) e2401452.
[157] X. Xie, W. Ma, Y. Zhan, et al., Curr. Drug Metab. 24 (2023) 315–326.
[158] S.Q. Zhang, Q. Fu, Y.J. Zhang, et al., Acta Pharmacol. Sin. 42 (2021) 1040–1054.
[159] S.H. Kim, K.R. Kim, D.R. Ahn, et al., ACS Nano 11 (2017) 9352–9359.
[160] H. Wang, Z. Wang, B. Li, et al., ACS Nano 19 (2025) 16032–16042.
[161] D. Mathur, K.E. Rogers, S.A. Díaz, et al., Nano Lett. 22 (2022) 5037–5045.
[162] A. Märcher, M.A.D. Nijenhuis, K.V. Gothelf, Angew. Chem. Int. Ed. 60 (2021) 21691–21696.
[163] L. Yang, H. Sun, Y. Liu, et al., Angew. Chem. Int. Ed. 57 (2018) 17294–17298.
[164] Z. Xia, P. Wang, X. Liu, et al., Biochemistry 55 (2016) 1326–1331.
[165] S.D. Perrault, W.M. Shih, ACS Nano 8 (2014) 5132–5140.
[166] H. Lee, S. Li, L. Liu, et al., Biosens. Bioelectron. 281 (2025) 117455.
[167] C. Yu, J. Zhao, F. Cheng, et al., Research 7 (2024) 0336.
[168] H. Dong, G. Song, D. Ma, et al., ACS Appl. Mater. Interfaces 13 (2021) 29416–29423.
[169] X. Wu, T. Wu, J. Liu, B. Ding, Adv. Healthc. Mater. 9 (2020) e2001046.
[170] F. Ding, Q. Mou, Y. Ma, et al., Angew. Chem. Int. Ed. 57 (2018) 3064–3068.
[171] J. Zhu, Y. Yang, W. Ma, et al., Nano Lett. 22 (2022) 2381–2390.
[172] W. Fu, C. You, L. Ma, et al., ACS Appl. Mater. Interfaces 11 (2019) 39525–39533.
[173] H. Mei, C. Sha, Q. Lv, et al., J. Control. Release 374 (2024) 466–477.
[174] S. Shi, Y. Chen, T. Tian, et al., Bone Res. 8 (2020) 6.
[175] W. Cui, X. Chen, J. Zhu, et al., Nanoscale 12 (2020) 17196–17202.
[176] J. Liu, T. Wu, X. Lu, et al., J. Am. Chem. Soc. 141 (2019) 19032–19037.
[177] Y.T.E. Chiu, H. Li, C.H.J. Choi, Small 15 (2019) e1805416.
[178] W. Sun, J. Wang, Q. Hu, et al., Sci. Adv. 6 (2020) eaba2983.
[179] D.J. Shiwarski, A.R. Hudson, J.W. Tashman, et al., Sci. Adv. 11 (2025) eadu5905.
[180] S.Y. Sonaye, P. Sikder, Tissue Eng. B: Rev. (2025), doi:10.1089/ten.teb.2025.0017.
[181] H. Wu, X. Lyu, M. Xu, et al., ACS Appl. Mater. Interfaces 17 (2025) 560–571.
[182] L. Yao, G. Zhang, Y. Wang, et al., Adv. Mater. 4 (2025) e2414336.
[183] Y. Wang, X. Lu, X. Wu, et al., Innovation 3 (2022) 100217.
[184] X. Shao, S. Lin, Q. Peng, et al., Small 12 (2017) 1602770.
[185] Z. Li, J. Zhou, C. Wang, et al., Chem. Sci. 14 (2023) 6654–6662.
[186] Y. Ban, L. Zhang, F. Zhou, et al., Anal. Chem. 97 (2025) 9248–9255.
[187] S. Zeng, J. Chen, C. Qi, et al., Anal. Chim. Acta 1351 (2025) 343903.
[188] Y. Li, J. Li, Y. Chang, Y. Lin, L. Sui, Chin. Chem. Lett. 35 (2024) 109414.
[189] T. Tian, T. Zhang, T. Zhou, et al., Nanoscale 9 (2017) 18402–18412.
[190] R. Jia, X. He, W. Ma, et al., Anal. Chem. 91 (2019) 15107–15113.
[191] Y. Wu, X. Xie, J. Zhu, L. Guan, M. Li, Int. J. Mol. Sci. 26 (2025) 477.
[192] T. Li, M. Li, Y. Wu, Y. Li, Biomolecules 14 (2024) 1447.
[193] Y. Yang, J. Yang, J. Zhu, et al., Bioact. Mater. 39 (2024) 191–205.
[194] Y. Qiu, Y. Qiu, W. Zhou, et al., Mater. Today Bio 31 (2025) 101486.
[195] M. Zhang, X. Zhang, T. Tian, et al., Bioact. Mater. 8 (2022) 368–380.
[196] M. Liu, W. Ma, D. Zhao, et al., ACS Appl. Mater. Interfaces 22 (2021) 25825–25835.
[197] Y. Lan, X. Li, B. Liu, et al., Drug Resist. Updat. 76 (2024) 101122.
[198] L. Fu, P. Li, J. Wu, et al., Regener. Biomater. 10 (2023) rbad085.
[199] Y. Zhao, S. Li, M. Feng, et al., Small 19 (2023) e2302326.
[200] W. Chen, H. Wang, Q. Sun, et al., Chin. Chem. Lett. 37 (2026) 111396.
[201] Y. Wen, M. Zhang, Y. Yao, et al., Chin. Chem. Lett. 34 (2023) 107549.